J Mol Model (2018) 24:346
https://doi.org/10.1007/s00894-018-3873-7

ORIGINAL PAPER

Binding of histamine to the H1 receptor—a molecular dynamics study

Christian A. Söldner[1] · Anselm H. C. Horn[1] · Heinrich Sticht[1]

Received: 14 August 2018 / Accepted: 5 November 2018
© Springer-Verlag GmbH Germany, part of Springer Nature 2018

Abstract

Binding of histamine to the G-protein coupled histamine H_1 receptor plays an important role in the context of allergic reactions; however, no crystal structure of the resulting complex is available yet. To deduce the histamine binding site, we performed unbiased molecular dynamics (MD) simulations on a microsecond time scale, which allowed to monitor one binding event, in which particularly the residues of the extracellular loop 2 were involved in the initial recognition process. The final histamine binding pose in the orthosteric pocket is characterized by interactions with Asp107$^{3.32}$, Tyr108$^{3.33}$, Thr194$^{5.43}$, Asn198$^{5.46}$, Trp428$^{6.48}$, Tyr431$^{6.51}$, Phe432$^{6.52}$, and Phe435$^{6.55}$, which is in agreement with existing mutational data. The conformational stability of the obtained complex structure was subsequently confirmed in 2 μs equilibrium MD simulations, and a metadynamics simulation proved that the detected binding site represents an energy minimum. A complementary investigation of a D107A mutant, which has experimentally been shown to abolish ligand binding, revealed that this exchange results in a significantly weaker interaction and enhanced ligand dynamics. This finding underlines the importance of the electrostatic interaction between the histamine ammonium group and the side chain of Asp107$^{3.32}$ for histamine binding.

Keywords G-protein coupled receptors (GPCRs) · Histamine · Molecular dynamics simulations · Metadynamics · Receptor–ligand interactions · Ligand binding · Allergic reactions

Introduction

Histamine is an endogenous tissue hormone and a key molecule for the regulation of arousal, inflammatory, and allergic reactions [1, 2]. Being extensively studied by medical research [1], it has been shown to stimulate lymphocyte activity, to facilitate the migration of immune cells, and to influence the behavior of granulocytes and mast cells [3, 4]. Histamine is known to be directly involved in the genesis of key symptoms observed in the context of allergic reactions such as an excessive production of mucus, sneezing, and pruritus [4]. The detection of histamine by a cell is mediated via four different G-protein coupled receptors (GPCRs): H_1, H_2, H_3, and H_4. All of them belong to the family of class-A GPCRs [5]. The histamine H_1 receptor is expressed in many different cell types, e.g., immune cells, neurons, as well as the smooth muscle cells of respiratory or intestinal epithelium as well as vascular endothelial cells [2]. It has been described to play a major role in type I hypersensitivity reactions: histamine released from mast cells binds to the receptor and leads to its activation [6], which is followed by a signal transduction via a G_q protein [5]. The activated heterotrimeric G-protein hydrolyses GTP to GDP and dissociates into its α and a dimeric $(\beta+\gamma)$ subunit. The α subunit binds to the enzyme phospholipase C (PLC), which is thereby triggered to catalyze the reaction of phosphoinositide-3,4-bisphosphate (PIP_2) to diacyl glycerol (DAG) and inositol 1,4,5-trisphosphate (IP_3). IP_3 leads to a release of the second messenger Ca^{2+} from the endoplasmatic reticulum, whereas DAG activates the protein kinase C (PKC) [7]. Both mechanisms convey changes in cellular metabolism and behaviour, which occur in the context of allergic processes. Due to its particular role for hypersensitivity reactions, the histamine H_1 receptor is a main target for anti-allergic drugs [8], which are used for the treatment of hay fever, conjunctivitis, allergic rhinitis, or anaphylactic

This paper belongs to the Topical Collection Tim Clark 70th Birthday Festschrift

Electronic supplementary material The online version of this article (https://doi.org/10.1007/s00894-018-3873-7) contains supplementary material, which is available to authorized users.

✉ Heinrich Sticht
Heinrich.Sticht@fau.de

[1] Bioinformatik, Institut für Biochemie, Emil-Fischer-Centrum, Friedrich-Alexander-Universität Erlangen-Nürnberg (FAU), Fahrstraße 17, 91054 Erlangen, Germany

Published online: 29 November 2018

shock [9]. The most relevant substances applied in therapy are inverse agonists of the H_1 receptor such as loratadine, olopatadine, or cetirizine [8].

In 2011, Shimamura et al. published a crystal structure of the histamine H_1 receptor bound to the small antagonist doxepin (PDB code 3RZE) [10]. However, there is to date no structure of a complex with the physiological ligand histamine available. The binding mode of histamine is so far more or less known due to a site-directed mutagenesis study by Ohta et al., which indicates that the residues Asp107$^{3.32}$, Thr194$^{5.43}$, and Asn198$^{5.46}$ (superscript numbers indicate Ballesteros–Weinstein numbering [11] of the respective residues) might be involved in ligand binding [12]. Before the crystal structure of the H_1 receptor became available, a first computational prediction for the histamine binding pocket was proposed based on a homology model [13]. Besides the three residues proposed by Ohta et al., this work suggested an involvement of Tyr108$^{3.33}$, Ser111$^{3.36}$, and Lys191$^{5.40}$. After the crystal structure was published, Panula et al. performed a docking study and suggested interactions of histamine with Asp107$^{3.32}$, Lys191$^{5.40}$, Thr194$^{5.43}$, Asn198$^{5.46}$, Tyr431$^{6.51}$, and Phe435$^{6.55}$ [14]. Taken together, these findings suggest that histamine binds to the orthosteric pocket of the H_1 receptor in a similar fashion like the antagonist doxepin.

To obtain further details of the histamine-H_1 receptor interaction, we applied a set of different molecular dynamics simulations: For the initial deduction of the histamine binding site, we performed three unbiased molecular dynamics (MD) simulations starting from an unbound ligand, one of which succeeded in placing the ligand in the orthosteric pocket. The obtained binding pose was subsequently validated by 2 μs equilibrium MD simulations and by a thermodynamic analysis based on metadynamics simulations. These simulations demonstrate the conformational stability of the detected binding mode, which also represents a minimum in the energy landscape. Moreover, we conducted analogous simulations of a D107A mutant, which reveal the role of a saltbridge between Asp107$^{3.32}$ and the histamine amino group for a stable binding position. Taken together, the results from our simulations allowed to refine the histamine binding mode and to identify the key interacting residues of the H_1 receptor. In the future, this information may be helpful for drug development or further functional studies of histamine receptors.

Methods

Simulations performed

To elucidate the binding site of histamine in the H_1 receptor, three simulations of at least 1 μs were performed, in which a single histamine molecule was placed $\approx$ 10 Å above the GPCR. The binding mode was afterwards verified by two independent 2-μs MD simulations. In addition, a D107A mutant was generated from the same starting structure and also simulated in two 2-μs simulation runs. An overview of the systems investigated is given in Table 1.

Preparation of histamine for MD simulations

Coordinates for histamine were downloaded from the PubChem database [15]. For the correct physiological protonation state (pK_a=9.7 for amino group, pK_a=5.8 for imidazole ring [16]), a third hydrogen atom was added to the amino group using Avogadro 1.1 [17]. *gaff* [18] atom types were assigned with the AmberTool `antechamber`. Partial charges for histamine were derived from a RESP/ESP fit with the RESP/ESP Charge Derive Server [19] using Firefly 7.1 [20, 21] and the base set RESP-C2 (HF/6-31G*//HF/6-31G*). The resulting final prep file is provided as the supplementary information of this paper (Online Resource 5). With `tleap` from AmberTools 17 [22], Amber coordinate and topology files for histamine were generated and then converted to the respective Gromacs formats with `amb2gmx.pl` as described in [23].

Preparation of the H_1 receptor starting structure

The structure of the histamine H_1 receptor was taken from PDB entry 3RZE [10]. The ligand doxepin and the T4 lysozyme used for crystallization were removed. The resulting gap between Cys221 and Leu405 was closed by an eight-residue spacer (sequence GSGSGSGS) using ModLoop [24, 25]. Additionally, the unresolved residues between His167 and Arg175 were completed with the native sequence. Since there were some missing terminal residues, an N-terminal acetyl and a C-terminal *N*-methyl capping group were added to the structure using Sybyl7.3 [26] to avoid artificial charges at the termini. The setup of the structure for the subsequent MD simulations was performed with `tleap`. Missing hydrogen atoms were added, the disulfide bridges mentioned in the PDB file were created, and *ff99SB* [27] parameters were assigned to the protein. The structure was then temporarily solvated in a TIP3P [28] waterbox (capped octahedron, minimum distance of 8 Å from the solute to the borders) with Cl^- counter ions for electrical neutralization. This was done to perform an initial energy minimization prior to membrane embedding in order to reduce steric tension in the starting structure. The energy minimization was conducted with `sander` from Amber17 and comprised 500 steps of *steepest descent* as well as 4500 steps of the *conjugate gradient* algorithm. Afterwards, water and ions were removed and `tleap` was run to generate new Amber coordinate and topology files for the minimized

Table 1 Overview of the unbiased MD simulations performed

System	Histamine	♯ runs	Simulation time	♯ DOPC	♯ H_2O	♯ Cl^-	♯ atoms
WT (initial binding)	unbound	3	1 μs, 3 μs, 3 μs	235	20,347	17	98,075
WT	bound	2	2 μs, 2 μs	235	20,347	17	98,075
D107A	bound	2	2 μs, 2 μs	235	20,346	18	98,071

All systems consist of either the wild-type (WT) or the mutant D107A histamine H_1 receptor, embedded into a dioleoylphosphatidylcholine (DOPC) bilayer and solvated in SPC water. The table contains the initial position of histamine, the number of independent runs performed, the simulation time per run, the number of DOPC and water molecules, the number of Cl^- ions for electrical neutralization, and the number of overall atoms in the respective system

protein structure using again parameters from the *ff99SB* force field. As described for histamine, the resulting files were then converted into Gromacs file formats with `amb2gmx.pl`. Based on the entry `3RZE` from the OPM database [29], the structure was then overlaid with a pre-equilibrated dioleoylphosphatidylcholine (DOPC) bilayer (*gaff* force field) [30] and solvated in SPC water [31]. This was done using an in-house Perl script, which minimized the sum of the squared z distances between the DOPC C1 atoms and the pseudoatom entries from the OPM entry by which the position of the extracellular and intracellular membrane layer are coded. Coordinates and topology of the solvated bilayer and the protein were then combined and the resulting structure was embedded into the membrane using the `gmx membed` [32] functionality of Gromacs 2016.5 [33]. An electrical neutralization of the system was performed by addition of Cl^- ions with `gmx genion`.

Then, a three-step energy minimization of the system was conducted, which comprised three steps in total. First, only water molecules and ions were minimized whereas all other atoms were restrained by the use of harmonic potentials with a force constant of 1000 kJ·mol^{-1}·nm^{-2} in x, y, and z direction. In the second step, the DOPC membrane and most of the H_1 receptor were minimized as well, only the Cα atoms were still restrained with the same force constant. Finally, the complete system including the Cα atoms was kept unrestrained. Every minimization phase was subdivided in a first part with the *steepest descent* algorithm and a second part with the *conjugate gradient* algorithm. The minimization was performed using `gmx mdrun` and terminated as soon as machine precision reached ($\approx$ a few thousands of steps).

In order to equilibrate the GPCR in the membrane, a series of 300 consecutive MD simulations (see Section "Molecular dynamics simulations" for details) of 100 ps length was performed. After each simulation, water molecules that had diffused between receptor and membrane were deleted using a self-written Perl script. During these equilibration simulations, position restraints with a force constant of 1000 kJ·mol^{-1}·nm^{-2} in x, y, and z direction were imposed on the protein backbone. After the 300 restrained simulations, an additional 2 μs free equilibration simulation of the system was performed to remove structural artifacts that might be due to the co-crystallization with the T4 lysozyme and the antagonist doxepin. For the histamine binding simulations, a single histamine molecule was added about 10 Å above the receptor on the extracellular side and an additional Cl^- ion was added to ensure electrical neutrality.

For the simulation of the D107A mutant, the Asp107$^{3.32}$ residue was exchanged for alanine with the Chimera `swapaa` command. Then, a new topology was created with `tleap` and converted into the Gromacs file format as described above.

Molecular dynamics simulations

All unbiased MD simulations were performed with Gromacs 2016.5 [33]. Periodic boundary conditions were applied in x, y, and z direction. The simulations were run at constant pressure and temperature (NpT ensemble) with surface-tension coupling. The reference surface tension was set to 1.1 nm·bar and the reference z pressure to 1 bar. The temperature was constantly held at 310 K with temperature coupling being achieved by a Berendsen thermostat [35] in three separate coupling groups for (i) solvent and ions, (ii) protein and ligand, and (iii) the DOPC membrane. A time step of 2 fs was used because bonds involving hydrogen atoms were constrained with the LINCS algorithm [36].

The analysis of the simulations was performed with `cpptraj` [37] from AmberTools 17. Contacts were defined between any atom pair (including hydrogen atoms) with a maximum distance of 5 Å, as described previously [38]. Plots were created with `gnuplot` [39], structure visualization was done with UCSF Chimera [34].

To assess the energy landscape of the obtained binding mode and to investigate the energetic effect of the D107A mutant, a well-tempered multiple walker metadynamics simulation was performed for both wild type and mutant according to a strategy established by Saleh et al. [40–42]. The metadynamics simulation was conducted using Gromacs 2016.3 [33] with the `plumed` 2.3.1 plugin [43].

As a collective variable (CV), we chose the z component of the distance between the conserved Trp428$^{6.48}$ Cα atom at the bottom of the orthosteric binding pocket and the histamine amino nitrogen atom. Methodical details are given in the supplementary information to this paper (Online Resource 1). Briefly, we initially conducted two metadynamics runs (one run for the wild type and one for the D107A mutant), which started from the bound state of histamine, in order to obtain a rapid ligand unbinding. From these initial simulations, 32 starting conformations were selected that were equidistantly distributed between the bound and the totally unbound state of histamine. Subsequently, for both wild type and mutant, multiple walker metadynamics simulations with a simulation time of $\approx$ 1500 ns (32$\times$48 ns) were conducted. The integration of the free energy landscape was performed with the `plumed` shell command.

Results and discussion

Determination of the histamine binding site

Molecular dynamics (MD) simulations, either in combination with enhanced sampling methods such as metadynamics or adaptive biasing force calculations or without external bias, have been successfully applied in the past in GPCR research to investigate ligand binding [41, 42, 44–47]. Therefore, we decided to use microsecond unbiased MD simulations for the identification of the histamine binding site in the present study. We performed a total of three simulations (1 μs each), in which histamine was placed above the H_1 receptor. Since only one of these simulations led to successful binding, the other two runs were extended to 3 μs. However, no binding event could be observed in those simulations despite this prolongation. Therefore, we will only discuss the successful run in more detail. As a measurement for the progress of binding, we chose two different parameters: (i) the z component of the distance between the histamine amino nitrogen atom and the Trp428$^{6.48}$ Cα atom (Fig. 1a), which is located directly below the binding pocket as described by Saleh et al. [40], and (ii) the number of contacts between histamine and the receptor (Fig. 1b). The binding process (movie in Online Resource 2) started after a simulation time of 600 ns and was complete at about 900 ns, taking 300 ns in total. As can be seen from Fig. 1b, it may be subdivided into three consecutive steps (visible as three plateaus). First, a small number of initial contacts ($<$ 100) was established mainly with charged residues of the ECL2 (Glu177, Asp178, Lys179, Glu181) (Fig. 1c). Then, a rapid increase to an intermediate phase of 300–400 contacts occurred when the ligand moved to the vestibule of the binding pocket. During this second step of the binding process, the ligand maintained interactions with residues of the ECL2 (Asp178, Lys179, Thr182, Tyr185) that form a kind of lid over the pocket (Fig. 1c). In addition, it contacted residues (such as Leu104$^{3.29}$, Lys191$^{5.40}$, His450$^{7.34}$, and Ile454$^{7.38}$), which belong to the outer parts of the transmembrane helices 3, 5, and 7. At about 900 ns of simulation time, the ligand descended further into the deep orthosteric binding pocket and established stable interactions with Asp107$^{3.32}$, Tyr108$^{3.33}$, Thr194$^{5.43}$, Asn198$^{5.46}$, Trp428$^{6.48}$, Tyr431$^{6.51}$, Phe432$^{6.52}$, and Phe435$^{6.55}$ (Fig. 1c).

This final binding mode (Fig. 2a, PDB file in Online Resource 6) is especially characterized by a saltbridge between one of the Asp107$^{3.32}$ Oδ atoms and the histamine ammonium group. Moreover, a hydrogen bond to Tyr431$^{6.51}$ was observed. Besides electrostatic interactions with the different tyrosine residues, hydrophobic interactions of the two phenylalanines Phe432$^{6.52}$ and Phe435$^{6.55}$ with the carbon atoms of the imidazole ring of histamine play a role as well.

When we analyzed the pathway from our initial binding simulation, we detected that especially the residues of the ECL2 formed contacts with histamine in the first phase of the binding process (Fig. 1c). This finding is in good agreement with the fact that this loop is already known to be particularly relevant for ligand recognition and ligand selectivity of class-A GPCRs [45, 48]. The entry of histamine happened through the crevice between the ECL2 and the transmembrane helices 5, 6, and 7 in a manner quite comparable to a binding pathway that was elucidated in an MD study for alprenolol at the β_2 adrenergic receptor [45].

Having reached the vestibule of the binding pocket, histamine interactions with the residues of the ECL2 remained important for a certain period of time until the ligand moved further inward into the orthosteric binding site (Fig. 1c). One role of the ECL2 for ligand binding is thus to catch the free ligand by means of a variety of charged residues and then to guide the ligand to the binding site as described in previous publications [49]. Such a role of the ECL2 as an enclosure for bound ligands has been discussed before [50]. Thus, our study is in line with previous publications [45, 48, 50] demonstrating that the ECL2 can be of high functional relevance and that its role is not limited on simply connecting two transmembrane helices with each other.

In summary, the comparison with the experimental data suggests that the present binding MD simulation has sampled a plausible entrance pathway to the orthosteric binding pocket. However, we are aware that a comprehensive investigation of ligand binding pathways, which will allow to assess the detailed role of individual residues in the binding process, requires the observations of more successful binding events. For example, Dror et al. performed 82

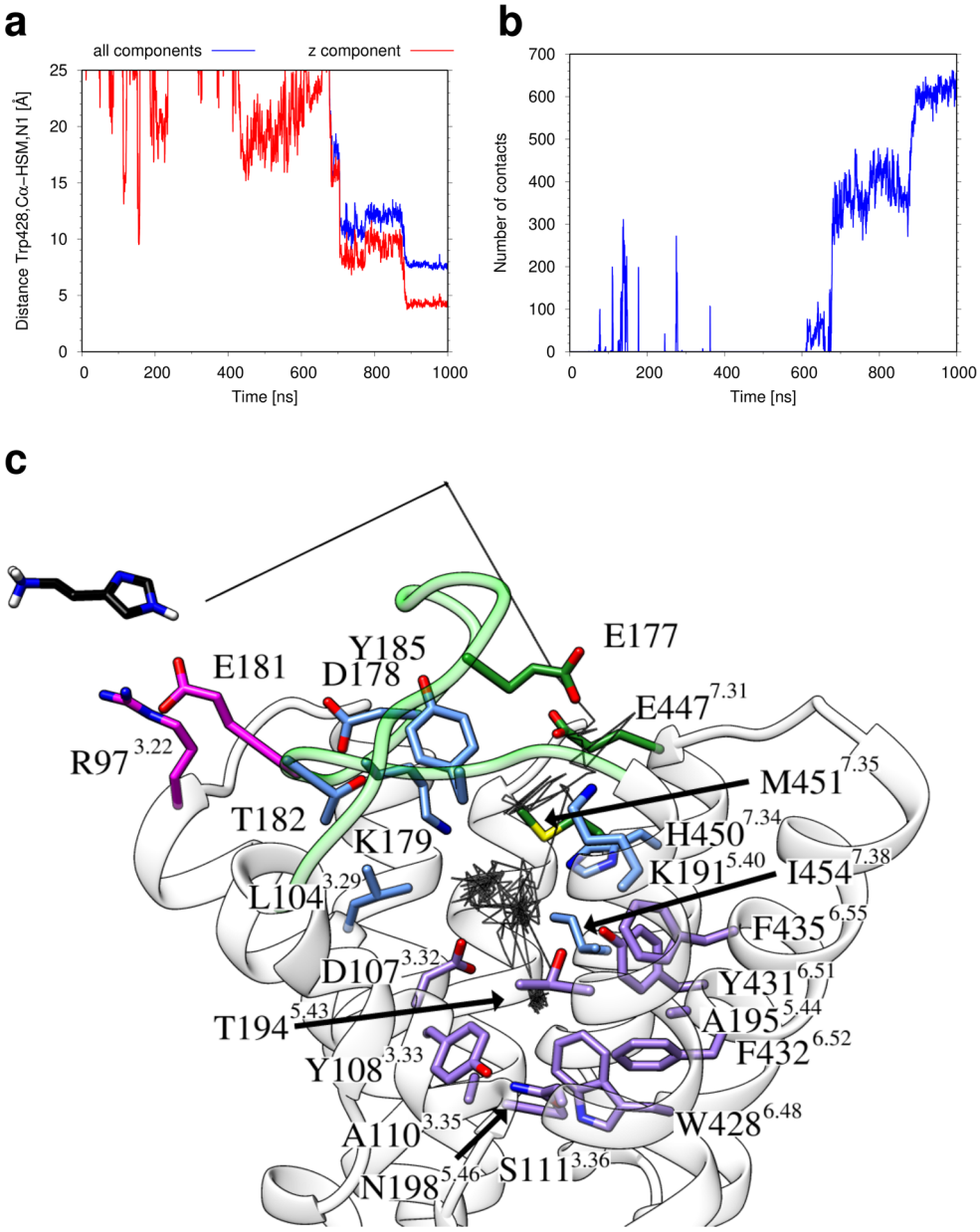

Fig. 1 Histamine binding to the H_1 receptor in an unbiased MD simulation. **a** Distance between the Trp428$^{6.48}$ Cα atom at the bottom of the orthosteric binding pocket and the histamine amino nitrogen atom as a function of simulation time. **b** Number of contacts between histamine and the H_1 receptor as a function of simulation time. **c** Structure of the upper part of the H_1 receptor. The backbone is depicted in *white*, all residues which are contacted by histamine during the binding process are shown as *sticks*. The color code indicates at what point in time they interact with histamine: first *magenta*, then *green*, *light blue*, and *violet* in the end. For better orientation, the backbone of the ECL2 is highlighted in *light green*. Histamine is shown as *black sticks* in a position at the beginning of the binding process. Its further movement during the following binding process is shown as a *black line* (one point every 10 ns)

simulations with 21 binding events to get a statistically sound data basis for such an analysis [45]. Thus, we consider our approach mainly as an alternative strategy to docking or enhanced sampling simulations to obtain a candidate binding mode for the ligand, which requires subsequent verification. We have performed this further verification by performing extended equilibrium MD simulations (Section "Stability of the histamine binding mode and role of D107 for the interaction"), by thermodynamic analyses (Section "Thermodynamics of the receptor–ligand interaction"), and by a comparison to previous experimental and computational data for the H_1 receptor (Section "Conclusions").

Comparison of the histamine binding mode with the doxepin-bound crystal structure

To date, the only available crystal structure for the H_1 receptor is a complex with the antagonist doxepin [10]. To investigate if our obtained binding mode involves similar interacting residues as this crystal structure, we performed an overlay of both structures (Fig. 2b). The result shows that the overall ligand position within the binding pocket is the same for histamine and doxepin. The two ligands have a similar orientation with their amino/amine nitrogen atom directing towards Asp107$^{3.32}$. To further characterize the similarities between the two binding modes, we compiled a

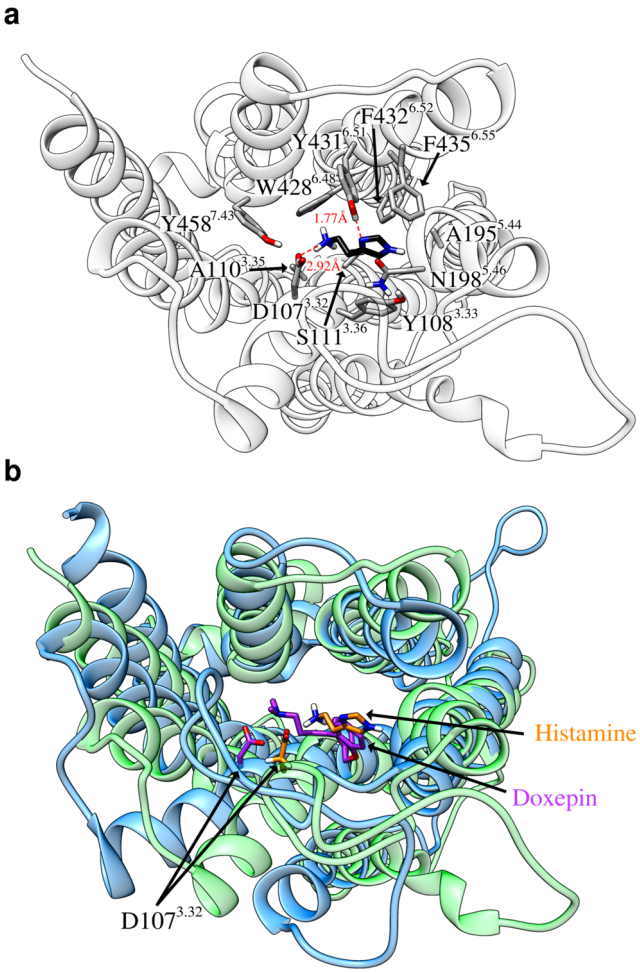

Fig. 2 Binding mode of histamine to the H_1 receptor from the last frame of the binding MD simulation. The H_1 receptor is shown from the extracellular side. **a** Overview of main interacting residues. The backbone is colored in *white* and the main residues which interact with histamine are displayed as *grey sticks*. Histamine is visualized as *black sticks*. The saltbridge between Asp107$^{3.32}$ and the histamine ammonium group as well as a hydrogen bond with Tyr431$^{6.51}$ are illustrated as *dashed red lines*. **b** Overlay of the histamine binding mode and the doxepin-bound crystal structure of the histamine H_1 receptor (PDB code 3RZE) [10]. The backbone of the crystal structure is colored in *blue*, doxepin (*Z* isomer from PDB 3RZE) and Asp107$^{3.32}$ are displayed as *violet sticks*. The backbone of the histamine-bound structure is colored in *green*, histamine and Asp107$^{3.32}$ are shown as *orange sticks*

Table 2 Comparison between the histamine binding mode obtained in the initial binding MD simulation and the doxepin binding mode from the crystal structure (PDB code 3RZE)

Residue	Histamine	Doxepin	GPCRdb mutations with effect on histamine/doxepin binding
Asp107$^{3.32}$	✓	✓	D107A (histamine: abolished or highly reduced [12, 52, 53], doxepin: 275× ⇓ [53]), D107E/N (histamine: abolished [12])
Tyr108$^{3.33}$	✓	✓	—
Ala110$^{3.35}$	✓	—	—
Ser111$^{3.36}$	✓	✓	S111A (histamine: 13× ⇓ [13]), S111C (histamine: 2× ⇑ [13]), S111T (histamine: no effect [13])
Thr112$^{3.37}$	—	✓	—
Ile115$^{3.40}$	—	✓	—
Trp158$^{4.57}$	—	✓	—
Lys179	—	✓	—
Lys191$^{5.40}$	✓	✓	K191A (histamine: 3-16× ⇓ [52, 54])
Thr194$^{5.43}$	✓	✓	T194A (histamine: 2-5× ⇓ [12, 54–57])
Ala195$^{5.44}$	✓	✓	—
Asn198$^{5.46}$	✓	✓	N198A (histamine: 16-775× ⇓ [12, 52, 55–57])
Phe199$^{5.47}$	—	✓	—
Phe424$^{6.44}$	—	✓	—
Trp428$^{6.48}$	✓	✓	—
Tyr431$^{6.51}$	✓	✓	—
Phe432$^{6.52}$	✓	✓	F432A (histamine: abolished [52])
Phe435$^{6.55}$	✓	✓	F435A (histamine: 3-40× ⇓ [52, 58])
Ile454$^{7.38}$	✓	✓	—
Tyr458$^{7.42}$	✓	✓	Y458A (histamine: 17× ⇓ [58], 1.3× ⇑ [52])

Residues were considered as interacting with histamine (✓) if a significant number of contacts was detected during the wild-type equilibrium simulations. For doxepin, all residues located in the crystal structure within 5 Å of the ligand were defined as binding. The fourth column contains information about the effect of experimental H_1 receptor mutations in the respective positions on histamine/doxepin binding. It is based on entries from the GPCRdb [51]

table (Table 2), which lists all interacting amino acids for the two ligands.

Besides Asp107$^{3.32}$, common interactions occurred with Tyr108$^{3.33}$, Ser111$^{3.36}$, Lys191$^{5.40}$, Thr194$^{5.43}$, Ala195$^{5.44}$, Asn198$^{5.46}$, Trp428$^{6.48}$, Tyr431$^{6.51}$, the two phenylalanines Phe432$^{6.52}$ and Phe435$^{6.55}$ as well as with Ile454$^{7.38}$ and Tyr458$^{7.42}$. Just one single residue, Ala110$^{3.35}$, was found to interact exclusively with histamine and not with doxepin. However, there were a couple of residues that were contacted by doxepin, but not involved in the binding of histamine (e.g., Thr112$^{3.37}$, Ile115$^{3.40}$, Trp158$^{4.57}$, Lys179, Phe199$^{5.47}$, and Phe424$^{6.44}$). This is most probably due to the fact that doxepin is larger compared to histamine, allowing it to reach residues that are located more distant from the center of the binding pocket. We also added information about mutagenesis studies with an effect on histamine or doxepin binding to Table 2 based on the information available from the GPCRdb [51]. These data will be discussed in more detail in Section "Conclusions".

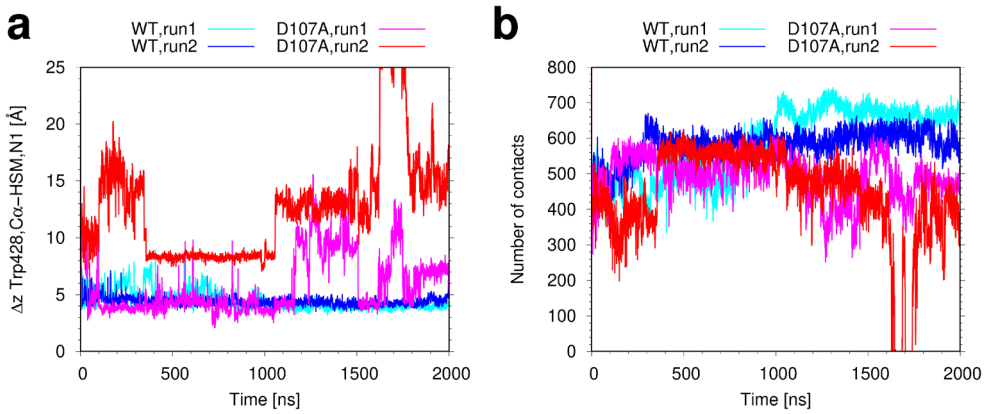

Fig. 3 Stability of the detected histamine binding mode for the wild-type H_1 receptor and the D107A mutant. **a** Distance between the Trp428$^{6.48}$ Cα atom at the bottom of the orthosteric binding pocket and the histamine amino nitrogen atom as a function of simulation time. **b** Number of contacts between histamine and the H_1 receptor as a function of simulation time

Stability of the histamine binding mode and role of D107 for the interaction

In order to test if the obtained binding mode remains stable and to investigate the relevance of the observed saltbridge (Fig. 2a), we performed subsequent 2 μs simulations of the wild-type receptor and a D107A mutant, in which the saltbridge is absent (two runs for each system). In case of the wild-type trajectories, we found that histamine remained constantly deep inside the binding pocket (movie in Online Resource 3, final structures from the two MD runs as PDB files in Online Resources 7, 8). This is also visible from the fact that the z distance between the histamine amino nitrogen atom and the Trp428$^{6.48}$ Cα atom remained constant over the entire trajectory (Fig. 3a). The number of contacts changed only slightly over the simulation time apart from some fluctuations and a small increase, which indicates a further enhancement of binding (Fig. 3b). In contrast, the runs of the D107A mutant showed both a lot more flexibility in the z distance of histamine from

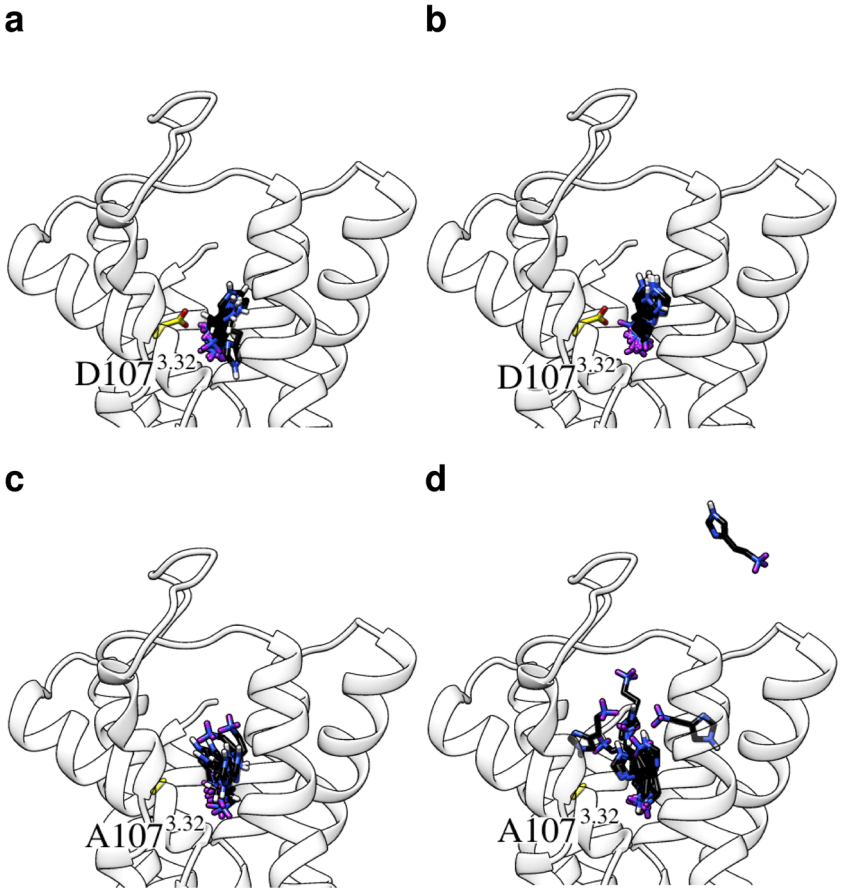

Fig. 4 Histamine flexibility within the binding pocket. Structure of the upper part of the H_1 receptor with an overlay of the histamine position for every 200 ns of simulation time. The backbone of the receptor is colored in *white*, and the residues Asp107$^{3.32}$/Ala107 are shown as *yellow sticks*. Histamine is shown as *black sticks* with nitrogen atoms colored in *blue*. The three protons of the NH_3^+ group are highlighted in *violet* to allow for an easier recognition of the orientation within the binding pocket. **a** Wild type, run1. **b** Wild type, run2. **c** D107A mutant, run1. **d** D107A mutant, run2

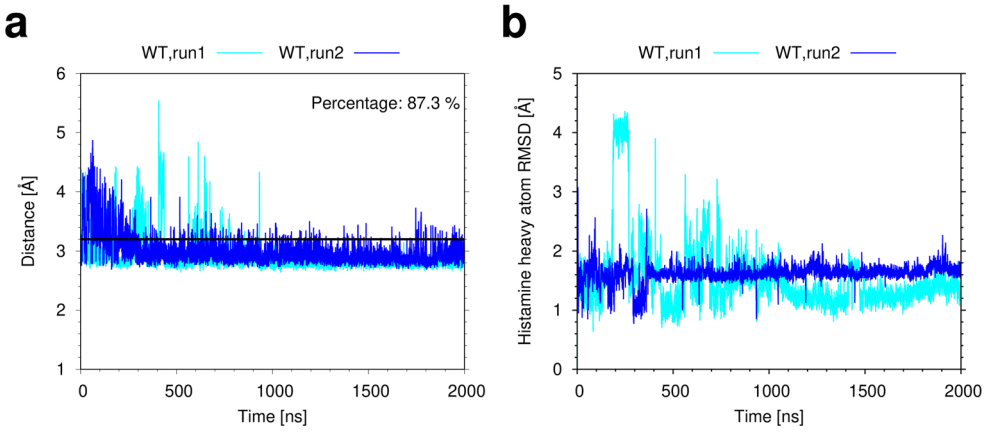

Fig. 5 Dynamics of histamine in the wild-type equilibrium MD simulations over time. **a** Saltbridge between the Asp107$^{3.32}$ Oδ atoms and the histamine amino nitrogen atom. To take into account the chemical equivalency of the two aspartate Oδ atoms, for every frame, the minimum distance out of the two possible atom combinations was calculated. **b** Root mean square deviation of the histamine heavy atoms. A translational and rotational fit was performed to the protein backbone for the analyzed frames to adjust the protein moiety

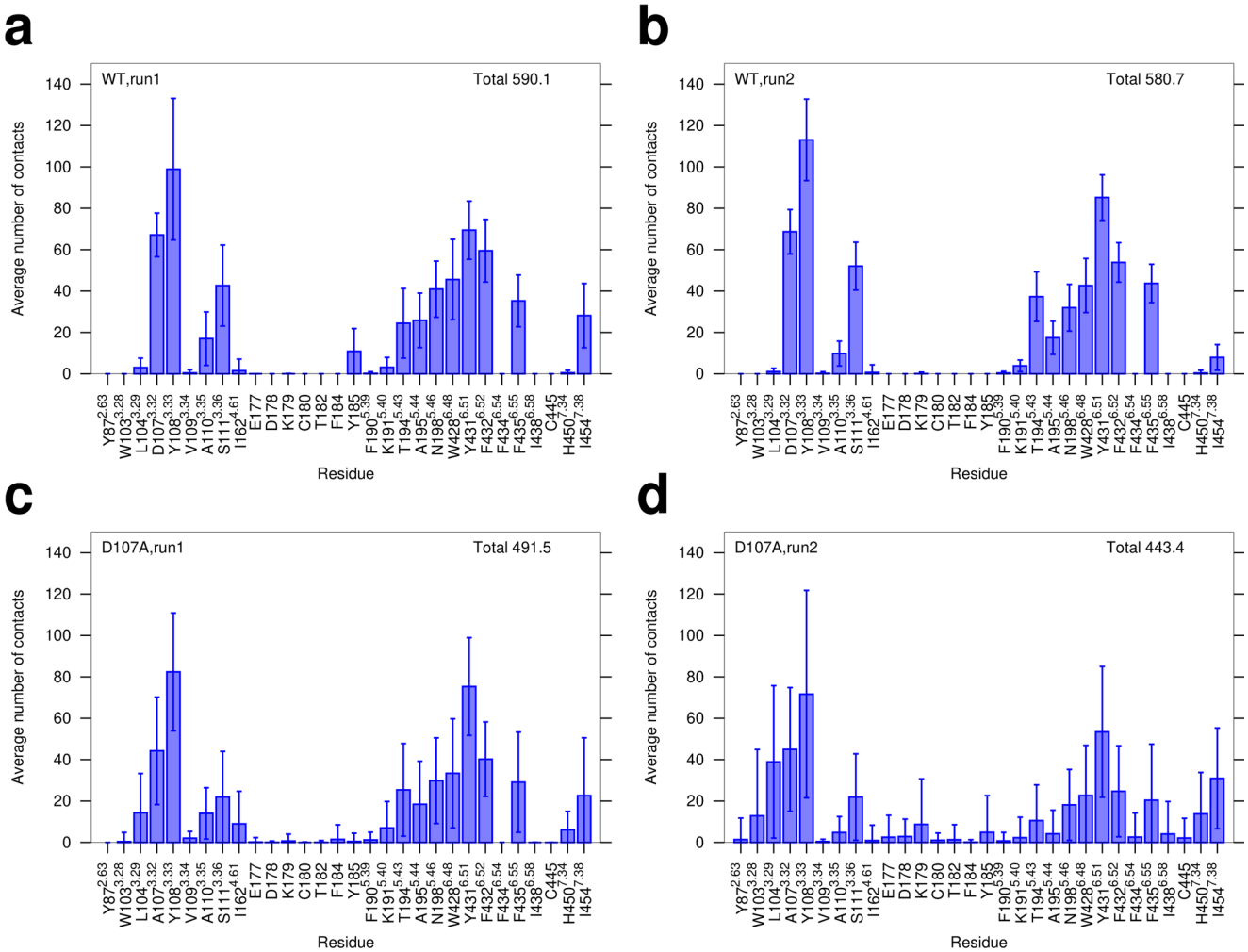

Fig. 6 Number of contacts between histamine and the H_1 receptor, dissected into individual amino acid residues. Averages per frame ± standard deviations. The diagrams contain all side chains of residues where on average at least one contact was detected per frame in at least one of the performed simulations. **a** Wild type, run1. **b** Wild type, run2. **c** D107A mutant, run1. **d** D107A mutant, run2

the bottom of the binding pocket (Fig. 3a). In run2, there was already at the beginning of the simulation (from about 150 to 400 ns) a phase where histamine moved from the orthosteric binding pocket towards the vestibule, which is visible as a plateau at about 10–15 Å. The ligand returned then into its initial position. However, in this second run, the z distance increased again at about 1 μs of simulation time reaching the same plateau before a complete dissociation of histamine occurred after about 1600 ns (movie in Online Resource 4). This becomes also evident from the fact that the number of contacts between histamine and the receptor decreased to zero at this point of simulation time (Fig. 3b). Subsequently, the unbound ligand moved through the solvent very quickly, forming only transient contacts with the protein (predominantly with the ECL2) until a re-association took place about 100 ns later. In the simulated time range, histamine went only back into the vestibule and did not re-enter the deep orthosteric region of the binding pocket although the remaining simulation time was longer than the time span observed for this descent in the initial binding simulation with the wild-type receptor.

The different dynamics of histamine between the wild-type and the mutant H_1 receptor can be visualized by an overlay of snapshots at different time points of the trajectories (Fig. 4). For the two wild-type runs (Fig. 4a, b), the general orientation of the ligand remained always

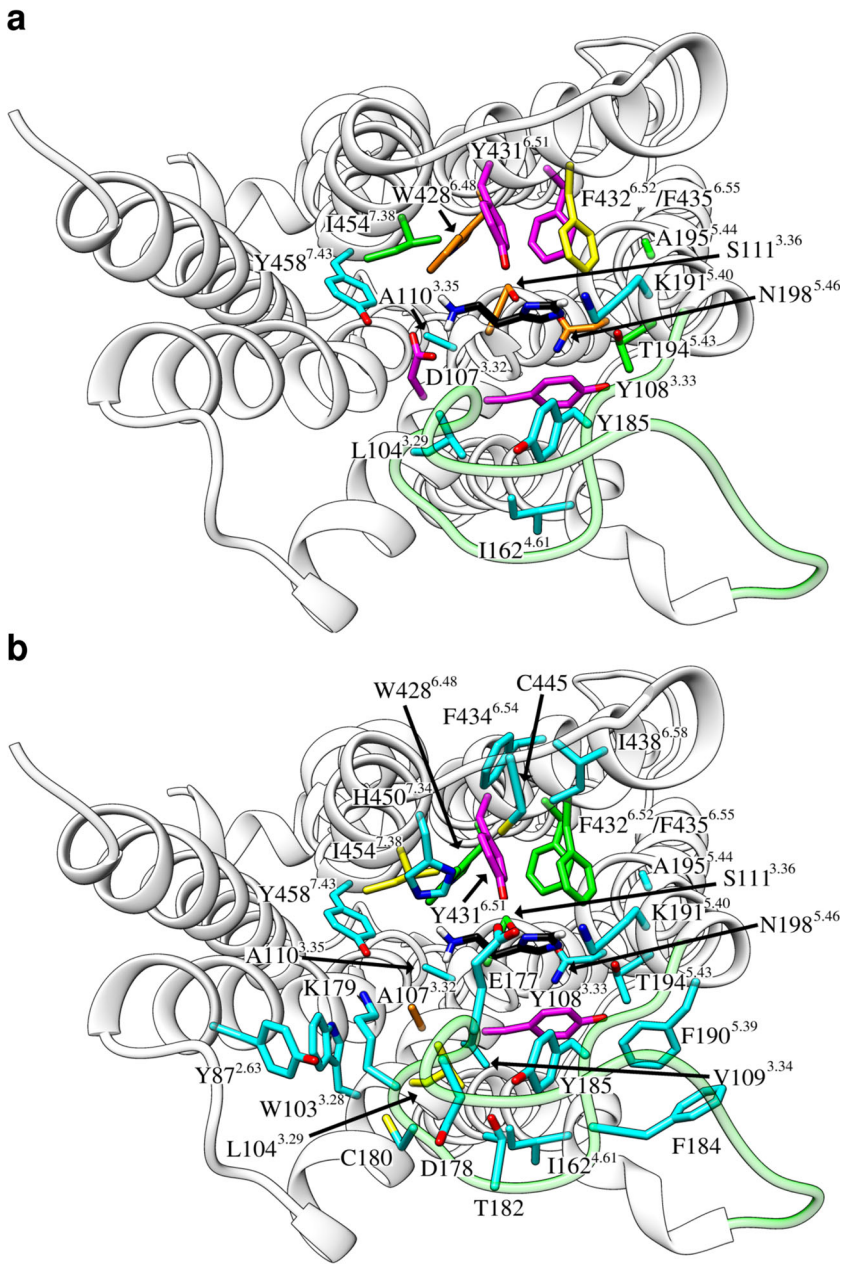

Fig. 7 H_1 receptor residues contacted by histamine. Structure of the H_1 receptor shown from the extracellular side. The backbone is colored in *white*. Histamine is shown as *black sticks*, all residues that interact with histamine are also depicted as *sticks* and colored according to the number of contacts they formed during the MD simulations: magenta>orange>yellow>green>cyan. For a better orientation, the backbone of the ECL2 is highlighted in *light green*. **a** Wild type, average over both runs. **b** D107A mutant, average over both runs

the same with the amino group directing towards the side chain of Asp107$^{3.32}$. A distance analysis revealed that the saltbridge between both charged groups persists over the majority (87 %) of the simulation time (Fig. 5a). The pronounced conformational stability becomes also apparent from a plot of the histamine root mean square deviation as a function of simulation time (Fig. 5b). In contrast, in case of the D107A mutant (Fig. 4c, d), histamine sometimes completely reversed its orientation, so that the amino group pointed towards the extracellular direction even if the ligand stayed within the orthosteric binding site (run1, Fig. 4c). In run2, there were because of the dissociation of histamine also snapshots in which the ligand was located in the vestibule or in the solvent outside the binding pocket.

To investigate the differences in histamine binding between wild-type and D107A mutant receptor in more detail, we performed an analysis of the average number of contacts between histamine and all protein residues, as shown in Fig. 6. Their localization in the 3D structure of the receptor is visualized in Fig. 7 with a color code for the relevance of the individual residues. The two wild-type runs (Fig. 6a, b) are very similar to each other regarding

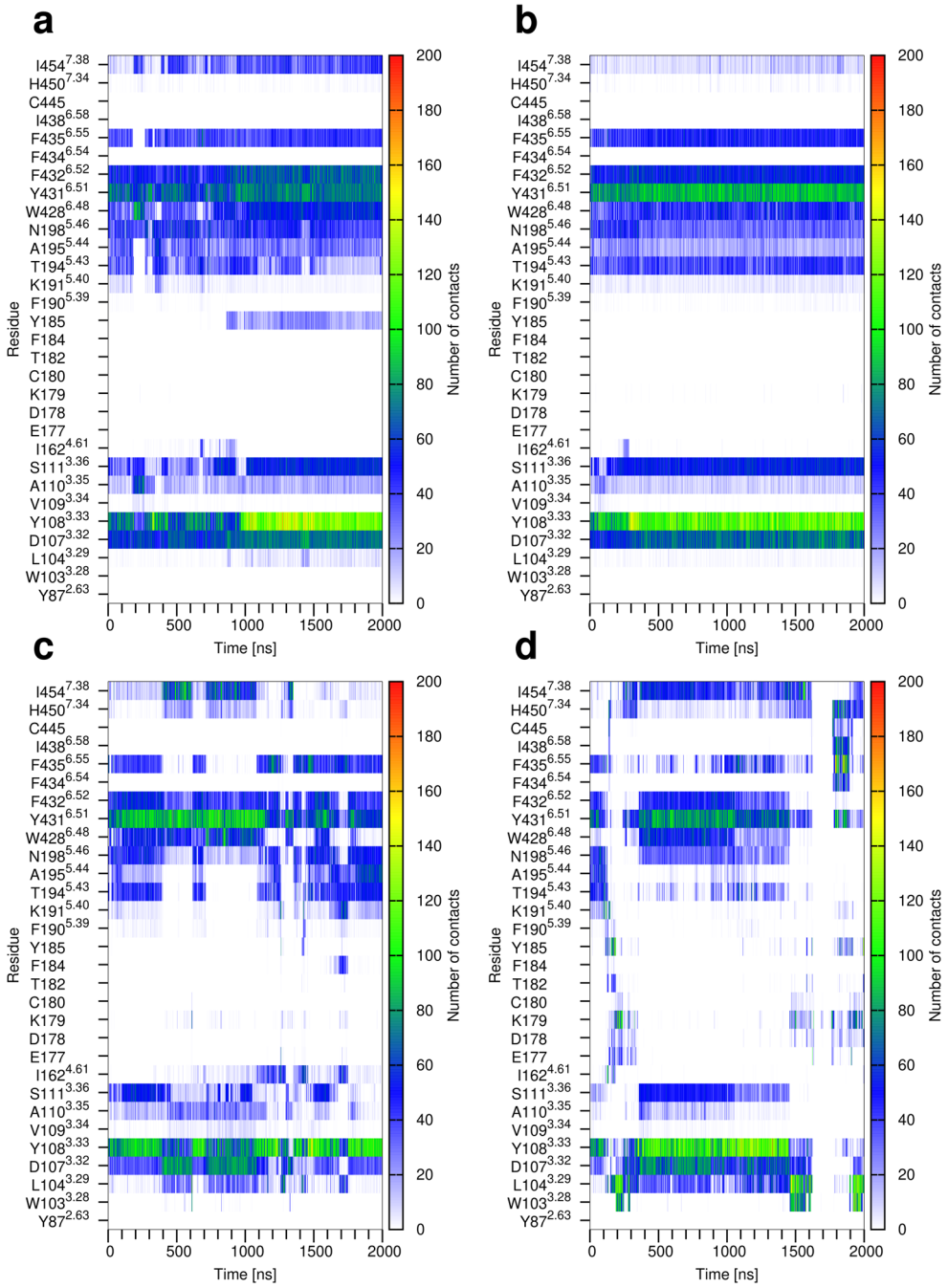

Fig. 8 Number of contacts between histamine and the H_1 receptor as a function of simulation time (x-axis) and the respective H_1 receptor residue (y-axis). The number of contacts is coded by color. **a** Wild type, run1. **b** Wild type, run2. **c** D107A mutant, run1. **d** D107A mutant, run2

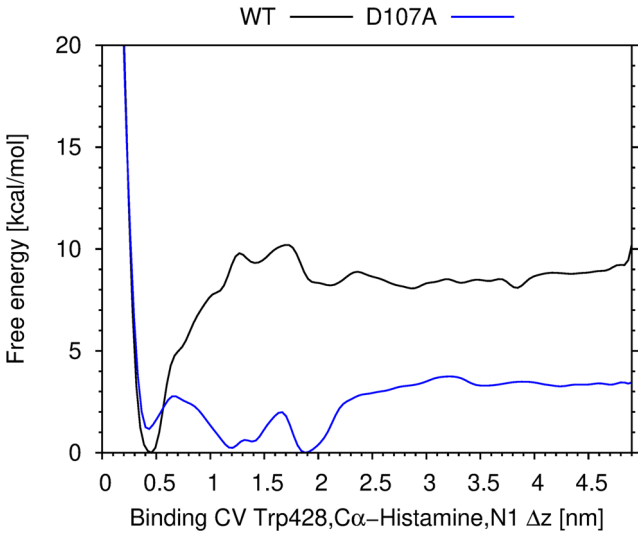

Fig. 9 Free energy of histamine binding as a function of the binding collective variable (z component of the distance between the Trp428$^{6.48}$ Cα atom and the histamine amino nitrogen atom). Result from multiple walker well-tempered metadynamics simulations (1500-ns cumulative simulation time per system)

the involved residues. Similar to the results from the end of the binding simulation (Fig. 2a), most contacts are observed with Tyr108$^{3.33}$, Asp107$^{3.32}$, Tyr431$^{6.51}$, Trp428$^{6.48}$ at the bottom of the binding pocket, and the two phenylalanines Phe432$^{6.52}$ and Phe435$^{6.55}$. The sum of all occurring interactions yields between 580 (run2) and 590 (run1) contacts per frame. For the D107A mutant runs (Fig. 6c, d), the main contacts are formed with the same residues. The alanine residue, by which Asp107$^{3.32}$ is replaced, forms about 40 contacts with the ligand compared to about 70 that were detected for the wild type. In fact, the numbers of contacts per residue are in general slightly lower for the mutant runs leading to a sum of 490 contacts in run1 and only 440 contacts in run2 where the transient dissociation occurred. Moreover, it becomes apparent that histamine interacts in case of the mutant receptor with a larger variety of different residues due to its higher flexibility within the binding pocket. This includes some minor interactions with the residues Val109$^{3.34}$, Phe184, and Phe190$^{5.39}$ in run1. For run2, there are some contacts with side chains from the ECL2 (residues 177-185, depicted in Fig. 7b), which arise when histamine leaves the orthosteric binding pocket, e.g., during the dissociation from the receptor and the subsequent re-association to the vestibule.

To verify if the contacts between histamine and the H_1 receptor remained stable for the wild-type simulations, we plotted the contact numbers as a function of the simulation time (Fig. 8a, b). The graphs demonstrate that there is only very limited variability: Most interactions are constantly present from the beginning until the end of the trajectory. For the D107A mutant, the same kind of analysis (Fig. 8c, d) shows that the contacts are much less stable. There are more breaks indicating that the ligand is not as tightly bound as in the wild-type receptor. For run2, it can be seen in Fig. 8d that the contacts, which occur with the residues of the ECL2, were not exclusively formed during the dissociation and re-association processes after 1500 ns of simulation time. In fact, there was already at the beginning (about 150-400 ns) a phase where the ECL2 was frequently contacted because histamine moved upward into the direction of the vestibule (Fig. 3a). Then, the ligand re-entered the orthosteric binding site so that no contacts with the ECL2 were formed for about 1 μs until the second movement to the vestibule and the consecutive dissociation took place. Interestingly, the ECL2 was not only contacted directly before the dissociation but also in an earlier phase followed by a return of histamine to the orthosteric binding pocket (Figs. 8d and 4d). This observation suggests that the ECL2, which forms a lid over the binding pocket, hampers the dissociation process holding the ligand back inside. The ECL2 was also important for the following re-association, especially Asp178 and Lys179. Besides these residues, the re-association was characterized by several predominantly hydrophobic interactions with the outer parts of transmembrane helix 6 and

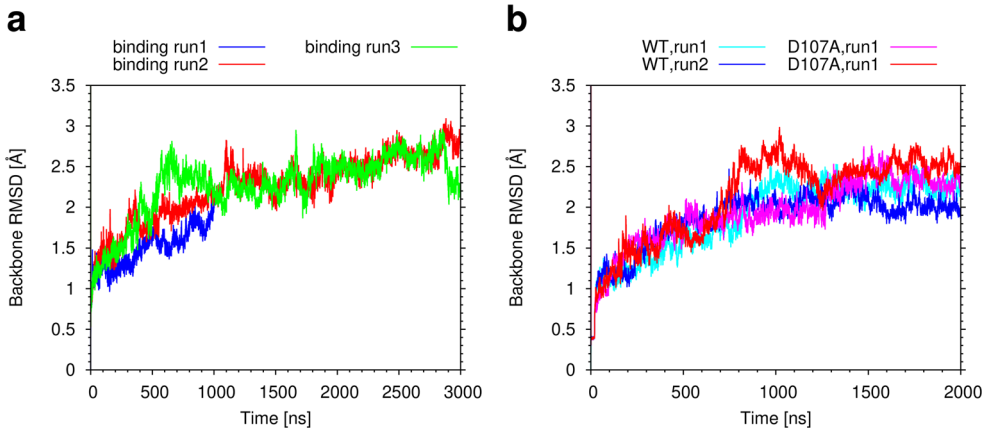

Fig. 10 Root mean square deviation of the H_1 receptor backbone as a function of simulation time. **a** Initial binding simulations. **b** Histamine-bound MD simulations

7 such as Phe432$^{6.52}$, Phe434$^{6.54}$, Phe435$^{6.55}$, Ile438$^{6.58}$ and His450$^{7.34}$. Together, these results indicate that the histamine amino group is strongly bound to Asp107$^{3.32}$ which also explains that the overall orientation of histamine in the binding pocket remains stable compared to the much higher dynamics in case of the D107A mutant (Fig. 4).

Thermodynamics of the receptor–ligand interaction

After the analysis of purely structural properties, we performed a complementing metadynamics simulation to investigate whether the binding mode from our unbiased MD study represents an energetic minimum. In order to explore how the energy landscape of the binding process is influenced by the D107A mutation, both the wild-type and the D107A mutant were studied. As a collective variable (CV), we chose in accordance with Saleh et al. [40] again the z component of the distance between the conserved Trp428$^{6.48}$ Cα atom at the bottom of the orthosteric binding pocket and the histamine amino nitrogen atom. Using the multiple walker technique with 32 different starting conformations between the bound and the totally unbound state (for details see methods section and Online Resource 1), we reached a cumulative simulation time of approximately 1500 ns (48 ns per walker) per system (wild-type or D107A mutant).

As shown in Fig. 9, the free energy landscape of the wild type has a pronounced global minimum at a CV value between 0.4 and 0.5 nm. This result is in good agreement with the distance observed in our long unbiased MD simulations (Fig. 3a), which suggests that the obtained binding position actually represents an energetic minimum. The D107A mutant, in contrast, displays only a weak local minimum at this CV value. This effect can most probably be attributed to the loss of electrostatic interactions between histamine and the charged Asp107$^{3.32}$ residue. The difference in the energy landscape of the D107A mutant also offers an energetic explanation for the higher dynamics of

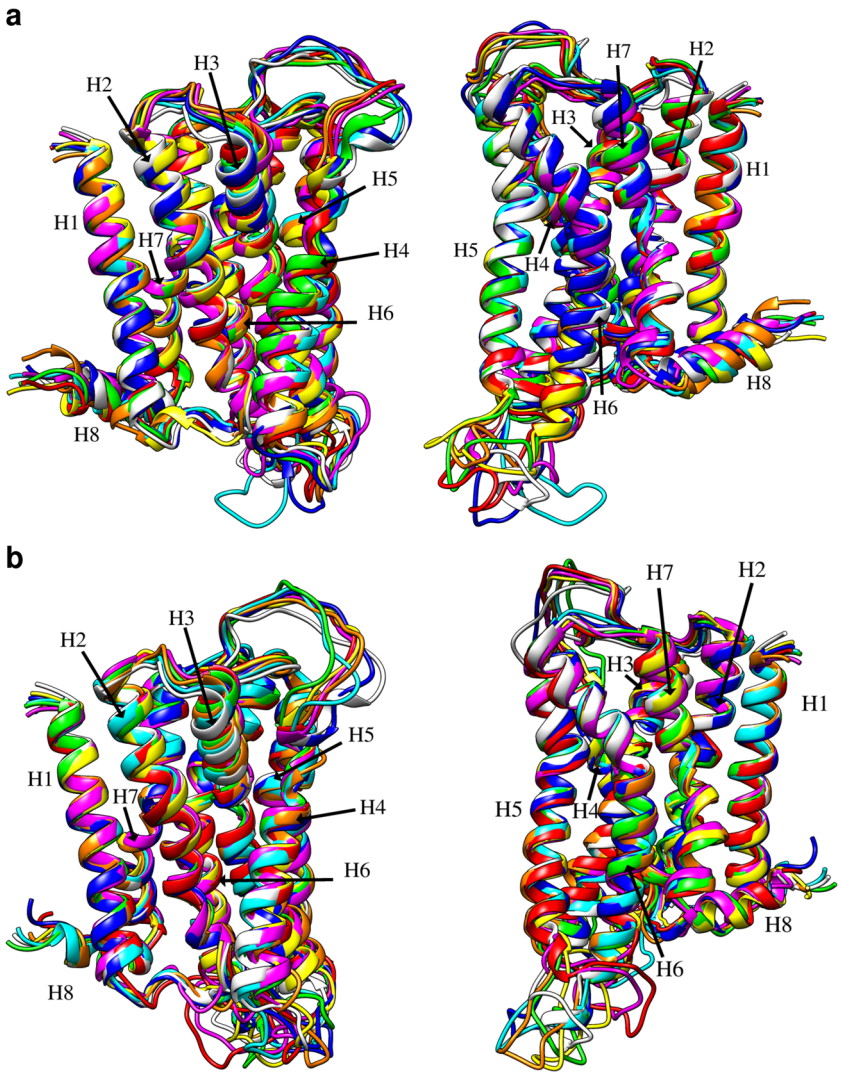

Fig. 11 Histamine H_1 receptor dynamics. Overlay of eight frames from equidistantly distributed time points in the trajectory in chronological order from white over blue, cyan, green, yellow, orange, and red to magenta. The receptor is shown in two different perspectives. **a** WT, run1. **b** D107A mutant, run1

histamine within the binding pocket of the mutant GPCR and the observed dissociation in one of the two unbiased MD runs.

Conformational stability of the H_1 receptor

Since the crystal structure we used for our MD study is stabilized by an antagonist and thus represents an inactive conformation, we also investigated the type of structural changes that occur upon histamine binding. In addition, we checked whether the D107A mutation has effects on the structure of the H_1 receptor. Therefore, we performed an analysis of the backbone root mean square deviation (RMSD) for the initial binding simulations (Fig. 10a) and the 2 μs simulations with bound histamine (Fig. 10b). The RMSD was generally rather low with about 2-3 Å at the end of the simulations. The final RMSD values for the D107A mutant are only marginally increased compared to the wild type (Fig. 10b), suggesting that no large structural rearrangements are triggered by the exchange of Asp107$^{3.32}$ for alanine. A structural overlay of frames at different time points of the trajectory (Fig. 11) shows that the general position of the transmembrane helices is rather stable for both wild type and mutant whereas the loops (especially the artificially constructed ICL 3) are more flexible.

In the context of agonist binding to an inactive GPCR, the question arises if there should be signs of receptor activation. Some activation mechanisms, which have been reported for class A GPCRs in the literature, include the disruption of the so-called ionic lock between helices 3 and 6, an outward rotation of transmembrane helix 6, as well as a downward movement of the Tyr$^{7.53}$ side chain (belongs to the NPxxY motif) [59–61]. The histamine H_1 receptor, however, lacks the ionic lock already in its inactive crystal structure [10], which makes it impossible to use it as an indicator for activation. From a structural overlay of the crystal structure and the two final structures of the wild-type MD runs with bound histamine (Fig. 12a),

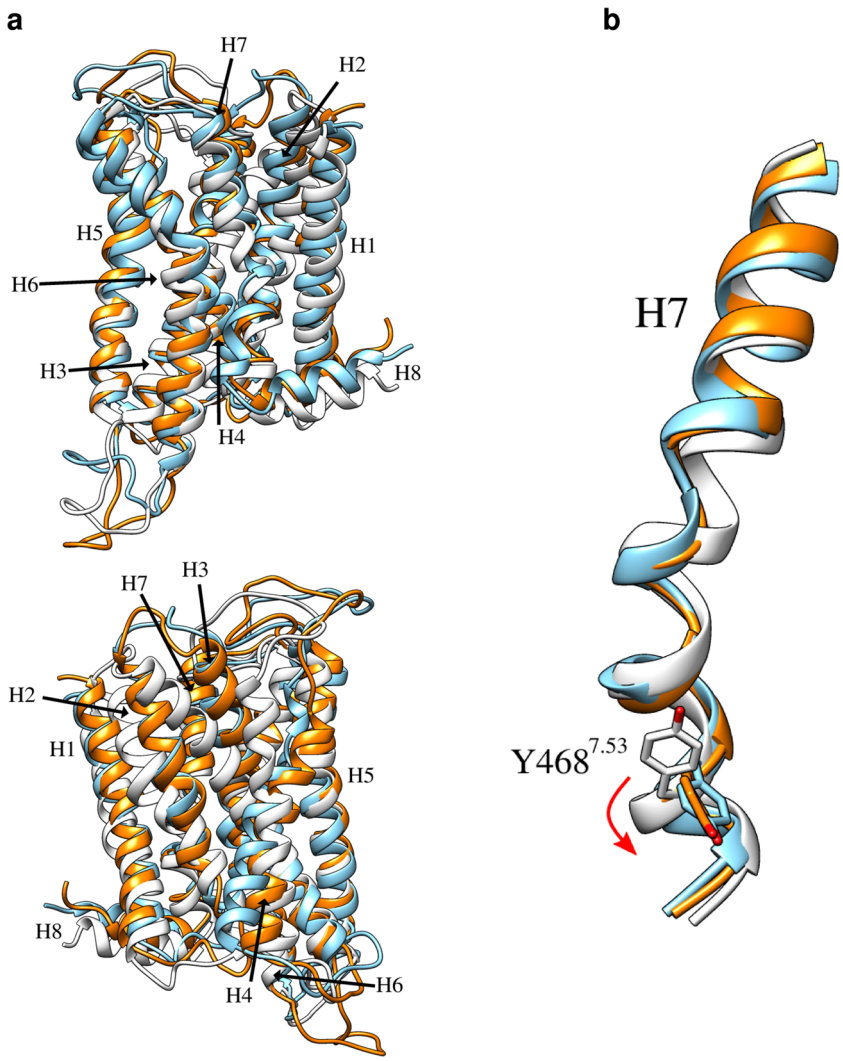

Fig. 12 Changes in the wild-type histamine H_1 receptor structure upon histamine binding. Structural overlays of the doxepin-bound crystal structure (*white*) and the final structures of the 2 μs wild-type MD simulations with bound histamine (*cyan* and *orange*). **a** Structural overlay for the whole receptor from two different perspectives. **b** Structural overlay of helix H7 demonstrating the downward rotation of the Tyr468$^{7.53}$ side chain

only a very slight outward rotation of helix 6 can be seen. However, we observed a downward movement of Tyr468$^{7.53}$ in helix 7 (Fig. 12b), which might be a first sign of a beginning activation process. The fact that there is no stronger evidence for receptor activation in our MD study can likely be explained by the time scale of the simulations or the absence of a bound G-protein. Data from the literature suggest that GPCR activation may rather take place on a millisecond than on a microsecond time scale [62]. Moreover, a full activation is at least for some GPCRs thought to require the stabilizing effect of a bound G-protein [46], which was not present in our simulations.

Conclusions

In this work, we used MD simulations to investigate histamine binding to the H_1 receptor. The following section is intended to set our observations in context with results from previous research. A comprehensive compilation of all residues that have been reported in the GPCRdb [51] to influence histamine binding is provided in Table 2.

In agreement with site-directed mutagenesis studies performed by Ohta et al. [12], we saw that the residues Asp107$^{3.32}$, Thr194$^{5.43}$, and Asn198$^{5.46}$ formed extensive contacts with histamine (Fig. 6). The saltbridge between Asp107$^{3.32}$ and the histamine amino group was particularly relevant for a stable binding mode because simulations of the D107A mutant showed much more flexibility for histamine and even a complete dissociation in one of two runs (Fig. 3, 4, Online Resources 3, 4). This result fits to an experimental investigation of D107A, D107N, and D107E mutations leading all to a complete abolishment of histamine binding [12]. Further studies have shown that the well-conserved Asp$^{3.32}$ residue in transmembrane helix 3 is of general importance for the binding of both agonists and antagonists to the whole group of biogenic amine receptors [53, 63, 64]. For the histamine H_1 receptor, this particular residue is known to be involved not only in interactions with histamine but also in the binding of doxepin from the crystal structure by Shimamura et al. [10], and several other antagonists such as KW-4679, acrivastine, or cetirizine [53, 65].

Besides residues Asp107$^{3.32}$, Thr194$^{5.43}$, and Asn198$^{5.46}$, a computational study, which was performed on a homology model before the H_1 receptor crystal structure became available, suggested a role of Tyr108$^{3.33}$, Ser111$^{3.36}$, and Lys191$^{5.40}$ for histamine binding [13]. In our simulations, we observed that especially the first two of these residues formed a high number of contacts with the ligand (Fig. 6). For Lys191$^{5.40}$, there exist also data from experimental studies indicating that a mutation to alanine leads to a moderate loss in histamine binding affinity [52, 54]. This is in line with the observation that this residue also contributed to binding in our MD trajectories, albeit only to a minor extent. Further residues, which were contacted in our MDs and for which experimental evidence is available, are the two phenylalanines Phe432$^{6.52}$ and Phe435$^{6.55}$ [52, 58]. Especially Phe432$^{6.52}$ seems to be of vital importance since a mutation of this residue was shown to abolish histamine binding [52]. Phe435$^{6.55}$, and additionally Tyr431$^{6.51}$, were also proposed as interacting residues in a later docking investigation by Panula et al. [14]. Our simulations revealed a high number of interactions with both of them.

Taken together, it can be concluded that the binding mode from our unbiased MD study is in rather good agreement with the results from previous investigations. We feel that the insights from our work may be useful for a better understanding of ligand binding at the H_1 receptor. In the future, this knowledge could be valuable for drug design given that the H_1 receptor plays an important role in the context of allergic reactions.

Acknowledgements The authors gratefully acknowledge the computer resources and support provided by the Erlangen Regional Computing Center (RRZE) and the Leibniz Rechenzentrum, Munich. C.A.S. would like to thank Jonas Kaindl from the Computer-Chemie-Centrum (CCC) of the FAU Erlangen-Nürnberg for fruitful discussions and valuable advice. This paper is dedicated to Prof. Tim Clark, an eminent computational chemist, on the occasion of his 70th birthday.

Author Contributions H.S. and C.A.S. conceived the study. A.H.C.H. and C.A.S. carried out the parametrization of histamine. C.A.S. performed the simulations and subsequent analyses. All authors interpreted the results and contributed to the manuscript.

Funding The study was funded by Deutsche Forschungsgemeinschaft (DFG) in the graduate school Graduiertenkolleg GRK1910. In addition, the work was supported by a grant of computer time on SuperMUC at the Leibniz Rechenzentrum, Munich (project pr74su).

Compliance with Ethical Standards

Conflict of interest The authors declare that they have no conflicts of interest.

References

1. Akdis CA, Simons FER (2006) Histamine receptors are hot in immunopharmacology. Eur J Pharmacol 533(1–3):69–76
2. Hill SJ (1990) Distribution, properties, and functional characteristics of three classes of histamine receptor. Pharmacol Rev 42(1):45–83
3. Akdis CA, Jutel M, Akdis M (2008) Regulatory effects of histamine and histamine receptor expression in human allergic immune responses. In: Chemical immunology and allergy, KARGER, pp 67–82. https://doi.org/10.1159/000154858
4. Canonica GW, Blaiss M (2011) Antihistaminic, anti-inflammatory, and antiallergic properties of the nonsedating second-generation antihistamine desloratadine: a review of the evidence. World Allergy Organ J 4(2):46–52. https://doi.org/10.1097/wox.0b013e3182093e19

5. Hill SJ, Ganellin CR, Timmerman H, Schwartz JC, Shankley NP, Young JM, Schunack W, Levi R, Haas HL (1997) International union of pharmacology. XIII. Classification of histamine receptors. Phamacol Rev 49(3):253–278
6. Simons FER (2004) Advances in H1-antihistamines. N Engl J Med 351(21):2203–2217. https://doi.org/10.1056/nejmra033121
7. Berridge MJ (1993) Inositol trisphosphate and calcium signalling. Nature 361(6410):315–325. https://doi.org/10.1038/361315a0
8. Monczor F, Fernandez N (2016) Current knowledge and perspectives on histamine H1 and H2 receptor pharmacology: functional selectivity, receptor crosstalk, and repositioning of classic histaminergic ligands. Mol Pharmacol 90(5):640–648. https://doi.org/10.1124/mol.116.105981
9. Simons FER, Simons KJ (2011) Histamine and H1-antihistamines: celebrating a century of progress. J Allergy Clin Immunol 128(6):1139–1150, e4. https://doi.org/10.1016/j.jaci.2011.09.005
10. Shimamura T, Shiroishi M, Weyand S, Tsujimoto H, Winter G, Katritch V, Abagyan R, Cherezov V, Liu W, Han GW, Kobayashi T, Stevens RC, Iwata S (2011) Structure of the human histamine H1 receptor complex with doxepin. Nature 475(7354):65–70. https://doi.org/10.1038/nature10236
11. Ballesteros JA, Weinstein H (1995) Integrated methods for the construction of three-dimensional models and computational probing of structure-function relations in G protein-coupled receptors. In: Methods in neurosciences. Elsevier, pp 366–428. https://doi.org/10.1016/s1043-9471(05)80049-7
12. Ohta K, Hayashi H, Mizuguchi H, Kagamiyama H, Fujimoto K, Fukui H (1994) Site-directed mutagenesis of the histamine H1 receptor: roles of aspartic acid 107, asparagine 198 and threonine 194. Biochem Biophys Res Commun 203(2):1096–1101
13. Jongejan A, Bruysters M, Ballesteros JA, Haaksma E, Bakker RA, Pardo L, Leurs R (2005) Linking agonist binding to histamine H1 receptor activation. Nat Chem Biol 1:98–103. https://doi.org/10.1038/nchembio714
14. Panula P, Chazot PL, Cowart M, Gutzmer R, Leurs R, Liu WLS, Stark H, Thurmond RL, Haas HL (2015) International union of basic and clinical pharmacology. XCVIII. Histamine receptors. Pharmacol Rev 67(3):601–655. https://doi.org/10.1124/pr.114.010249
15. Kim S, Thiessen PA, Bolton EE, Chen J, Fu G, Gindulyte A, Han L, He J, He S, Shoemaker BA, Wang J, Yu B, Zhang J, Bryant SH (2015) PubChem substance and compound databases. Nucleic Acids Res 44(D1):D1202–D1213. https://doi.org/10.1093/nar/gkv951
16. Paiva TB, Tominaga M, Paiva ACM (1970) Ionization of histamine, *N*-acetylhistamine, and their iodinated derivatives. J Med Chem 13(4):689–692. https://doi.org/10.1021/jm00298a025
17. Hanwell MD, Curtis DE, Lonie DC, Vandermeersch T, Zurek E, Hutchison GR (2012) Avogadro: an advanced semantic chemical editor, visualization, and analysis platform. J Cheminformatics 4(1):17. https://doi.org/10.1186/1758-2946-4-17
18. Wang J, Wolf RM, Caldwell JW, Kollman PA, Case DA (2004) Development and testing of a general amber force field. J Comput Chem 25(9):1157–1174. https://doi.org/10.1002/jcc.20035
19. Vanquelef E, Simon S, Marquant G, Garcia E, Klimerak G, Delepine JC, Cieplak P, Dupradeau FY (2011) R.E.D. server: a web service for deriving RESP and ESP charges and building force field libraries for new molecules and molecular fragments. Nucleic Acids Res 39(suppl):W511–W517. https://doi.org/10.1093/nar/gkr288
20. Granovsky AA (2010) Firefly version 7.1. http://classic.chem.msu.su/gran/firefly/index.html
21. Schmidt MW, Baldridge KK, Boatz JA, Elbert ST, Gordon MS, Jensen JH, Koseki S, Matsunaga N, Nguyen KA, Su S, Windus TL, Dupuis M, Montgomery JA (1993) General atomic and molecular electronic structure system. J Comput Chem 14(11):1347–1363. https://doi.org/10.1002/jcc.540141112
22. Case DA, Cerutti D, Cheatham IIIT, Darden T, Duke R, Giese T, Gohlke H, Goetz A, Greene D, Homeyer N, Izadi S, Kovalenko A, Lee T, LeGrand S, Li P, Lin C, Liu J, Luchko T, Luo R, Mermelstein D, Merz K, Monard G, Nguyen H, Omelyan I, Onufriev A, Pan F, Qi R, Roe DA, Roitberg A, Sagui C, Simmerling C, Botello-Smith W, Swails J, Walker R, Wang J, Wolf R, Wu X, Xiao L, York D, Kollman P (2017) AMBER 2017. University of California, San Francisco
23. Mobley DL, Chodera JD, Dill KA (2006) On the use of orientational restraints and symmetry corrections in alchemical free energy calculations. J Chem Phys 125(8):084902. https://doi.org/10.1063/1.2221683
24. Fiser A, Do RKG, Sali A (2000) Modeling of loops in protein structures. Protein Sci 9(9):1753–1773. https://doi.org/10.1110/ps.9.9.1753
25. Fiser A, Sali A (2003) ModLoop: automated modeling of loops in protein structures. Bioinformatics 19(18):2500–2501. https://doi.org/10.1093/bioinformatics/btg362
26. Tripos International, St Louis, MO, USA (2006) Sybyl 7.3
27. Hornak V, Abel R, Okur A, Strockbine B, Roitberg A, Simmerling C (2006) Comparison of multiple Amber force fields and development of improved protein backbone parameters. Proteins 65(3):712–725. https://doi.org/10.1002/prot.21123
28. Jorgensen WL, Chandrasekhar J, Madura JD, Impey RW, Klein ML (1983) Comparison of simple potential functions for simulating liquid water. J Chem Phys 79(2):926–935. https://doi.org/10.1063/1.445869
29. Lomize MA, Pogozheva ID, Joo H, Mosberg HI, Lomize AL (2011) OPM database and PPM web server: resources for positioning of proteins in membranes. Nucleic Acids Res 40(D1):D370–D376. https://doi.org/10.1093/nar/gkr703
30. Siu SWI, Vácha R, Jungwirth P, Böckmann RA (2008) Biomolecular simulations of membranes: physical properties from different force fields. J Chem Phys 128(12):125103. https://doi.org/10.1063/1.2897760
31. Toukan K, Rahman A (1985) Molecular-dynamics study of atomic motions in water. Phys Rev B 31(5):2643–2648. https://doi.org/10.1103/physrevb.31.2643
32. Wolf MG, Hoefling M, Aponte-Santamaría C, Grubmüller H, Groenhof G (2010) g_membed: efficient insertion of a membrane protein into an equilibrated lipid bilayer with minimal perturbation. J Comput Chem 31(11):2169–2174. https://doi.org/10.1002/jcc.21507
33. Berendsen H, van der Spoel D, van Drunen R (1995) GROMACS: a message-passing parallel molecular dynamics implementation. Comput Phys Commun 91(1-3):43–56. https://doi.org/10.1016/0010-4655(95)00042-e
34. Pettersen EF, Goddard TD, Huang CC, Couch GS, Greenblatt DM, Meng EC, Ferrin TE (2004) UCSF Chimera–a visualization system for exploratory research and analysis. J Comput Chem 25(13):1605–1612. https://doi.org/10.1002/jcc.20084
35. Berendsen HJC, Postma JPM, van Gunsteren WF, DiNola A, Haak JR (1984) Molecular dynamics with coupling to an external bath. J Chem Phys 81(8):3684–3690. https://doi.org/10.1063/1.448118
36. Hess B, Bekker H, Berendsen HJC, Fraaije JGEM (1997) LINCS: a linear constraint solver for molecular simulations. J Comput Chem 18(12):1463–1472
37. Roe DR, Cheatham TE (2013) PTRAJ and CPPTRAJ: software for processing and analysis of molecular dynamics trajectory data. J Chem Theory Comput 9:3084–3095. https://doi.org/10.1021/ct400341p
38. Söldner CA, Horn AHC, Sticht H (2018) Interaction of glycolipids with the macrophage surface receptor Mincle – a systematic

molecular dynamics study. Sci Rep 8:1. https://doi.org/10.1038/s41598-018-23624-8
39. Williams T, Kelley C et al (2018) Gnuplot 4.6: an interactive plotting program, 2012. http://www.gnuplot.info
40. Saleh N, Ibrahim P, Saladino G, Gervasio FL, Clark T (2017) An efficient metadynamics-based protocol to model the binding affinity and the transition state ensemble of G-protein-coupled receptor ligands. J Chem Inf Model 57(5):1210–1217. https://doi.org/10.1021/acs.jcim.6b00772
41. Saleh N, Kleinau G, Heyder N, Clark T, Hildebrand PW, Scheerer P (2018a) Binding, thermodynamics, and selectivity of a non-peptide antagonist to the Melanocortin-4 receptor. Front Pharmacol, 9. https://doi.org/10.3389/fphar.2018.00560
42. Saleh N, Hucke O, Kramer G, Schmidt E, Montel F, Lipinski R, Ferger B, Clark T, Hildebrand PW, Tautermann CS (2018b) Multiple binding sites contribute to the mechanism of mixed agonistic and positive allosteric modulators of the cannabinoid CB1 receptor. Angewandte Chemie Int Edn 57(10):2580–2585. https://doi.org/10.1002/anie.201708764
43. Bonomi M, Branduardi D, Bussi G, Camilloni C, Provasi D, Raiteri P, Donadio D, Marinelli F, Pietrucci F, Broglia RA, Parrinello M (2009) PLUMED: a portable plugin for free-energy calculations with molecular dynamics. Comput Phys Commun 180(10):1961–1972. https://doi.org/10.1016/j.cpc.2009.05.011
44. Saleh N, Saladino G, Gervasio FL, Haensele E, Banting L, Whitley DC, de Oliveira-Santos JS, Bureau R, Clark T (2016) A three-site mechanism for agonist/antagonist selective binding to vasopressin receptors. Angewandte Chemie Int Edn 55(28):8008–8012. https://doi.org/10.1002/anie.201602729
45. Dror RO, Pan AC, Arlow DH, Borhani DW, Maragakis P, Shan Y, Xu H, Shaw DE (2011) Pathway and mechanism of drug binding to G-protein-coupled receptors. Proc Natl Acad Sci 108(32):13118–13123. https://doi.org/10.1073/pnas.1104614108
46. Clark T (2017) G-protein coupled receptors: answers from simulations. Beilstein J Org Chem 13:1071–1078. https://doi.org/10.3762/bjoc.13.106
47. Marino KA, Filizola M (2017) Investigating small-molecule ligand binding to G protein-coupled receptors with biased or unbiased molecular dynamics simulations. In: Methods in molecular biology. Springer, New York, pp 351–364. https://doi.org/10.1007/978-1-4939-7465-8_17
48. Peeters M, van Westen G, Li Q, IJzerman A (2011) Importance of the extracellular loops in G protein-coupled receptors for ligand recognition and receptor activation. Trends Pharmacol Sci 32(1):35–42. https://doi.org/10.1016/j.tips.2010.10.001
49. Strasser A, Wittmann HJ, Seifert R (2017) Binding kinetics and pathways of ligands to GPCRs. Trends Pharmacol Sci 38(8):717–732. https://doi.org/10.1016/j.tips.2017.05.005
50. Wheatley M, Wootten D, Conner M, Simms J, Kendrick R, Logan R, Poyner D, Barwell J (2012) Lifting the lid on GPCRs: the role of extracellular loops. Br J Pharmacol 165(6):1688–1703. https://doi.org/10.1111/j.1476-5381.2011.01629.x
51. Påndy-Szekeres G, Munk C, Tsonkov TM, Mordalski S, Harpsøe K, Hauser AS, Bojarski AJ, Gloriam DE (2017) GPCRdb in 2018: adding GPCR structure models and ligands. Nucleic Acids Res 46(D1):D440–D446. https://doi.org/10.1093/nar/gkx1109
52. Bruysters M, Pertz HH, Teunissen A, Bakker RA, Gillard M, Chatelain P, Schunack W, Timmerman H, Leurs R (2004) Mutational analysis of the histamine H1-receptor binding pocket of histaprodifens. Eur J Pharmacol 487(1–3):55–63. https://doi.org/10.1016/j.ejphar.2004.01.028
53. Nonaka H, Otaki S, Ohshima E, Kono M, Kase H, Ohta K, Fukui H, Ichimura M (1998) Unique binding pocket for KW-4679 in the histamine H1 receptor. Eur J Pharmacol 345(1):111–117. https://doi.org/10.1016/s0014-2999(97)01620-8
54. Gillard M (2002) Binding characteristics of cetirizine and levocetirizine to human H1 histamine receptors: Contribution of Lys191 and Thr194. Mol Pharmacol 61(2):391–399. https://doi.org/10.1124/mol.61.2.391
55. Bakker RA (2004) 8R-lisuride is a potent stereospecific histamine H1-receptor partial agonist. Molec Pharmacol 65(3):538–549. https://doi.org/10.1124/mol.65.3.538
56. Leurs R, Smit M, Tensen C, Terlaak A, Timmerman H (1994) Site-directed mutagenesis of the histamine H1-receptor reveals a selective interaction of asparagine207 with subclasses of H1-receptor agonists. Biochem Biophys Res Commun 201(1):295–301. https://doi.org/10.1006/bbrc.1994.1701
57. Moguilevsky N, Varsalona F, Guillaume JP, Noyer M, Gillard M, Daliers J, Hénichart JP, Bollen A (1995) Pharmacological and functional characterisation of the wild—type and site—directed mutants of the human H1 histamine receptor stably expressed in CHO cells. J Recept Signal Transd 15(1-4):91–102. https://doi.org/10.3109/10799899509045210
58. Cordova-Sintjago TC, Fang L, Bruysters M, Leurs R, Booth RG (2012) Molecular determinants of ligand binding at the human histamine H1 receptor: site-directed mutagenesis results analyzed with ligand docking and molecular dynamics studies at H1 homology and crystal structure models. J Chem Pharm Res 4(6):2937–2951
59. Kobilka BK (2007) G protein coupled receptor structure and activation. Biochimica et Biophysica Acta (BBA) - Biomembranes 1768(4):794–807. https://doi.org/10.1016/j.bbamem.2006.10.021
60. Kimata N, Reeves PJ, Smith SO (2015) Uncovering the triggers for GPCR activation using solid-state NMR spectroscopy. J Magn Reson 253:111–118. https://doi.org/10.1016/j.jmr.2014.12.014
61. Venkatakrishnan AJ, Deupi X, Lebon G, Heydenreich FM, Flock T, Miljus T, Balaji S, Bouvier M, Veprintsev DB, Tate CG, Schertler GFX, Babu MM (2016) Diverse activation pathways in class a GPCRs converge near the G-protein-coupling region. Nature 536(7617):484–487. https://doi.org/10.1038/nature19107
62. Vilardaga JP, Bünemann M, Krasel C, Castro M, Lohse MJ (2003) Measurement of the millisecond activation switch of G protein-coupled receptors in living cells. Nat Biotechnol 21(7):807–812. https://doi.org/10.1038/nbt838
63. Schwartz TW, Rosenkilde MM (1996) Is there a lock for all agonist keys in 7TM receptors? Trends Pharmacol Sci 17:6. https://doi.org/10.1016/0165-6147(96)10017-1
64. Strader CD, Fong TM, Graziano MP, Tota MR (1995) The family of G-protein coupled receptors. FASEB J 9(9):745–754
65. Wieland K, Laak AMT, Smit MJ, Kühne R, Timmerman H, Leurs R (1999) Mutational analysis of the antagonist-binding site of the histamine H1 receptor. J Biol Chem 274(42):29994–30000. https://doi.org/10.1074/jbc.274.42.29994

Supplementary Information

Binding of histamine to the H_1 receptor – a molecular dynamics study

Christian A. Söldner, Anselm H. C. Horn, and Heinrich Sticht✉

Supplementary Methods – Metadynamics

We performed a well-tempered multiple walker metadynamics simulation of histamine and the wild type H_1 receptor to investigate if the binding mode from our unbiased MD study represents an energetic minimum. Moreover, the D107A mutant receptor was studied to explore how the energy landscape of the binding process is influenced by this mutation. Our simulations were conducted according to an established strategy published by Saleh *et al.* [1–3].
As a starting structure for the metadynamics analysis, we used the histamine-receptor complex which had been obtained in the initial histamine binding simulation. A PDB file of this structure is provided in online resource 6. All metadynamics simulations were conducted using Gromacs 2016.3 [4] with the `plumed` 2.3.1 plugin [5].

1 Collective variable

The DOPC membrane in our simulations was arranged parallel to the xy plane of the coordinate system. To investigate the histamine binding process to the H_1 receptor, we could thus use the z component of the distance between the histamine amino nitrogen atom and the Cα atom of the residue Trp428$^{6.48}$ at the bottom of the binding pocket (Fig. S1). The fact that only the z component is used ensures free sampling in x/y direction.

2 Limitation of sampled space – funnel and walls

To limit sampling to the space relevant for ligand dissociation, the binding path was confined in both x/y and z direction with potential walls (schematic depiction in Fig. S1). A lower wall was defined at $z_{\text{low}} = 0.3$ nm, an upper wall at $z_{\text{up}} = 4.9$ nm. These walls (`plumed` commands `UPPER_WALLS`, `LOWER_WALLS`) have the form of harmonic potentials, but are only applied to the outside:

$$\text{Bias}_{\text{up}}(z) = \begin{cases} 0 & \text{for } z < z_{\text{up}} \\ \kappa \cdot (z - z_{\text{up}})^2 & \text{for } z \geq z_{\text{up}} \end{cases} \tag{1}$$

$$\text{Bias}_{\text{low}}(z) = \begin{cases} \kappa \cdot (z - z_{\text{low}})^2 & \text{for } z \leq z_{\text{low}} \\ 0 & \text{for } z > z_{\text{low}} \end{cases} \tag{2}$$

The parameter κ was chosen as $\kappa = 1500\ \text{kJ} \cdot \text{mol}^{-1} \cdot \text{nm}^{-2}$.
To achieve faster convergence, a bell-shaped funnel was applied in x/y direction. The funnel was chosen parallel to the z axis; its centre in x/y direction is equal to the coordinates of the Trp428$^{6.48}$ Cα atom. Near the ligand binding site, the funnel has a large diameter of 4.8 nm to avoid a bias in this region which is especially important for the binding affinity. For high z coordinates, the funnel narrows to a diameter of 1.6 nm to reduce sampling at far outside positions within the solvent in which

✉ Heinrich.Sticht@fau.de

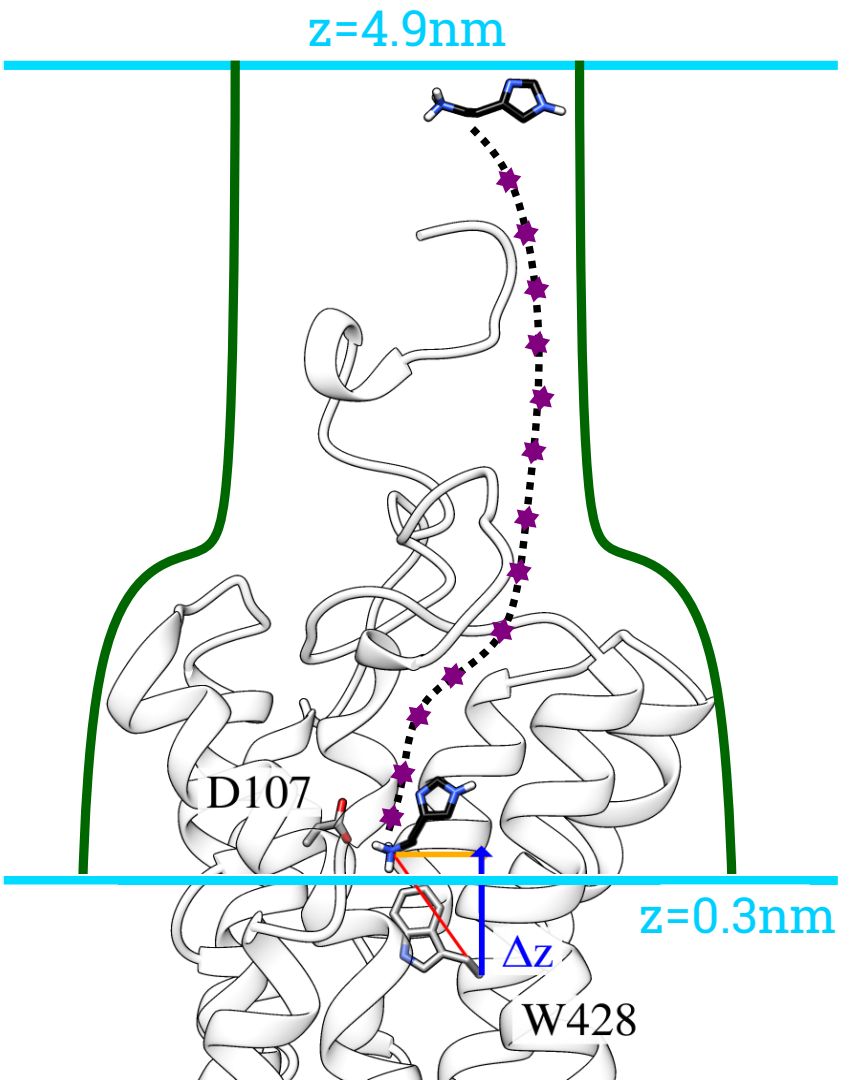

Figure S1: Schematic overview of the conducted multiple walker metadynamics simulations. A detailed description is provided in the main text. The figure shows a part of the histamine H_1 receptor with Trp428$^{6.48}$ and Asp107$^{3.32}$ depicted as grey sticks. Histamine (carbon atoms as black sticks, nitrogen atoms blue) is depicted both in its binding position and in an unbound state. The distance between the amino nitrogen atom of histamine and the Cα atom of Trp428$^{6.48}$ is shown in red, the z component, which was used as collective variable, is depicted as blue arrow. In a first short metadynamics simulation, a rapid unbinding of histamine was triggered. From the observed unbinding path (black dashed line), 32 equidistant starting conformations (violet stars) were chosen. Based on these structures, a multiple walker metadynamics run was performed. The space accessible to histamine is confined in x/y direction by a funnel (2D projection shown in green). In z direction, it is limited by a lower and an upper wall (visualized in cyan).

no ligand-protein interactions occur any more. The radius $R(z)$ of the funnel is given as a function of the z coordinate as

$$R(z) = \frac{d}{1 + \exp\left(m \cdot (z - w)\right)} + r_1, \tag{3}$$

where r_1 is the limit for high values of z (ligand totally unbound), d the difference between r_1 and the limit of the radius for low values of z (ligand inside binding pocket), and w the inflection point

of the function (Fig. S2a). The parameter m influences the steepness of the transition between the wide lower and the tight upper region. We used the values d=1.6 nm, r_1=0.8 nm, m=10 nm^{-1}, and w=2.8 nm for our study.

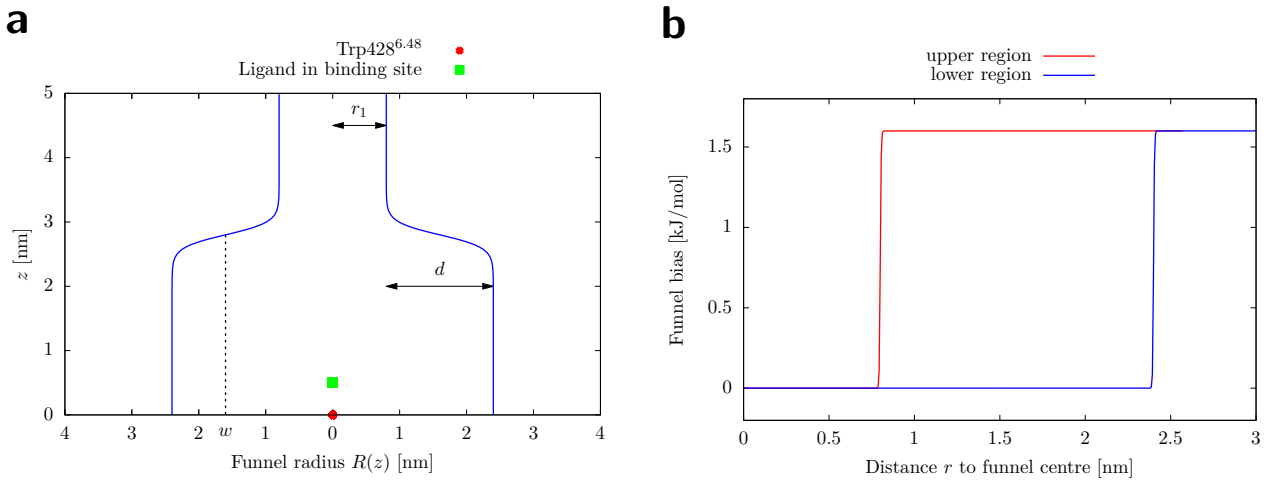

Figure S2: Funnel and bias at the funnel borders. (**a**) 2D model visualizing the funnel which confines the sampled space in x/y directions. The funnel radius is shown on the horizontal axis, the z coordinate (reaction coordinate) on the vertical axis. The funnel is arranged parallel to the z axis. (**b**) Bias potential, which shows a step-like rise at the funnel borders, as a function of the distance to the funnel centre. An exact description of the two subfigures is provided in the main text.

Depending on the xy projection $r(x, y)$ of the distance between the amino nitrogen atom of histamine and the funnel centre, which is given as

$$r(x, y) = \sqrt{x^2 + y^2}, \tag{4}$$

a funnel bias potential

$$\text{Funnel bias}(x, y, z) = h \cdot \left(1 - \frac{1}{1 + \exp\left(\lambda \cdot (r(x, y) - R(z))\right)}\right) \tag{5}$$

is introduced. This potential rises similar to a step function from 0 to its upper limit h once the border of the funnel is crossed (Fig. S2b). The steepness of this potential is controlled with the parameter λ. The values applied in this work were h=100 kJ·mol^{-1} and λ=500.

3 Metadynamics protocol and parameters

The metadynamics protocol used in this paper comprised two consecutive steps. First, starting from the final structure of the initial histamine binding simulation (H_1 receptor with bound histamine), a short 25 ns well-tempered metadynamics simulation with bias factor 50, gaussian width 0.1 and an initial bias height of 7 kJ $\cdot$ mol^{-1} was performed. The time step was 2 fs and the simulation temperature was 310 K. A new bias potential was added every 500 steps. The relatively high bias resulted in a rapid dissociation of the ligand.

From the trajectory of this initial simulation, 32 equidistant conformations along the unbinding path were extracted (schematic representation in Fig. S1). With a reduced bias factor of 20 and a lower initial bias height of 5 kJ $\cdot$ mol^{-1}, a multiple walker metadynamics simulation was conducted. The 32 simulations were run in parallel and the bias was shared between the different replicas. Afterwards, the free energy landscape was calculated using the `plumed` shell command.

References

[1] Noureldin Saleh, Passainte Ibrahim, Giorgio Saladino, Francesco Luigi Gervasio, and Timothy Clark. "An Efficient Metadynamics-Based Protocol To Model the Binding Affinity and the Transition State Ensemble of G-Protein-Coupled Receptor Ligands". In: *J. Chem. Inf. Model.* 57.5 (May 2017), pp. 1210–1217. DOI: 10.1021/acs.jcim.6b00772.

[2] Noureldin Saleh, Gunnar Kleinau, Nicolas Heyder, Timothy Clark, Peter W. Hildebrand, and Patrick Scheerer. "Binding, Thermodynamics, and Selectivity of a Non-peptide Antagonist to the Melanocortin-4 Receptor". In: *Frontiers in Pharmacology* 9 (June 2018). DOI: 10.3389/fphar.2018.00560.

[3] Noureldin Saleh, Oliver Hucke, Gert Kramer, Esther Schmidt, Florian Montel, Radoslaw Lipinski, Boris Ferger, Timothy Clark, Peter W. Hildebrand, and Christofer S. Tautermann. "Multiple Binding Sites Contribute to the Mechanism of Mixed Agonistic and Positive Allosteric Modulators of the Cannabinoid CB1 Receptor". In: *Angewandte Chemie International Edition* 57.10 (Feb. 2018), pp. 2580–2585. DOI: 10.1002/anie.201708764.

[4] H.J.C. Berendsen, D. van der Spoel, and R. van Drunen. "GROMACS: A message-passing parallel molecular dynamics implementation". In: *Computer Physics Communications* 91.1-3 (Sept. 1995), pp. 43–56. DOI: 10.1016/0010-4655(95)00042-e.

[5] Massimiliano Bonomi, Davide Branduardi, Giovanni Bussi, Carlo Camilloni, Davide Provasi, Paolo Raiteri, Davide Donadio, Fabrizio Marinelli, Fabio Pietrucci, Ricardo A. Broglia, and Michele Parrinello. "PLUMED: A portable plugin for free-energy calculations with molecular dynamics". In: *Computer Physics Communications* 180.10 (Oct. 2009), pp. 1961–1972. DOI: 10.1016/j.cpc.2009.05.011.